High-Resolution THz Transmission and Reflection Measurements and Consequent Understanding of Resonant Hole-Arrays

Yuping Yang and Daniel R. Grischkowsky, *Fellow, IEEE*

***Abstract*—We report high-resolution THz-TDS characterization of the transmission and reflection of a thin metal hole-array in optical contact with a 10 mm thick high-resistivity Si plate. It was found that the red-shift of the $[\pm 1, 0]$ spoof surface-plasmon (SSP) transmission peak from the Wood's anomaly valley indicates the coupling strength of the SSP wave to the metal surface due to the filling factor and shape of the holes, and that the red-shift provides a measurement of the SSP wave velocity. Our measurements of the amplitude transmission peak, and the corresponding reflection dip, of the hole-array agreed with numerical simulation to an accuracy of ± 2 GHz, and the measured phase was in good agreement with simulation. However, our reflection measurements showed a second unexplained dip at the frequency of Wood's anomaly.**

***Index Terms*—Hole-arrays, spoof surface plasmons, surface plasmons, THz-TDS.**

I. Introduction

THE transmission of electromagnetic waves through hole-arrays and metal meshes in thick and thin metal sheets has been studied both theoretically and experimentally for developing narrow band frequency filters and high contrast cut-off and high-pass filters. For example, there are the pioneering far-infrared experiments and theories on metallic meshes of R. Ulrich [1], and the general and comprehensive theory of the transmission through a conducting metal sheet perforated periodically with apertures by Chen [2]. More recent work describes both experimental and theoretical studies on far-infrared filters using arrays of very short waveguides [3], mid-IR filters using arrays of conducting elements [4], and an early example, of a THz-TDS measurement of a hole array on relatively thick metal sheet [5].

The first observation of the resonance enhanced transmission of light through a periodic sub-wavelength hole-array in a metal sheet by Ebbesen [6] has attracted significant attention due to the surface-plasmon (SP) physical mechanisms and the possible applications in a variety of fields. At THz frequencies sub-wavelength periodic hole-arrays and other periodic structures are easily fabricated by simple lithographic techniques. Also, the frequency-independent, high-conductivity of metals at THz frequencies enables duplication of microwave phenomena on 100 to 1000 times smaller physical scale. Although there have been many measurements of the THz transmission through thin metal film hole-arrays, under many different conditions of film material, film thickness, geometrical symmetry, lattice constant, hole size, and hole shape [7]–[13], few studies have been devoted to a fundamental physical understanding of the hole-array transmission and reflection. For THz-TDS studies, this is due in part to the limited time scan determined by the reflection from the backside of the sample wafer, typically 0.5 mm thick. An attempt to eliminate this problem and obtain higher resonance Q-factors and low loss in THz periodic arrays, by perforating sub-wavelength apertures on free-standing metal foils, had only limited success due to fabrication and dimension limitations [13]. Although the THz reflection of a metal hole array has been studied with thin film coverings [14], the corresponding phase of the reflection has not yet been measured.

The relatively new concept of spoof surface plasmons (SSP) [15]–[18] is essential to understand the microwave and THz measurements on patterned metal surfaces, due to their frequency-independent, high conductivity given by the handbook dc value. Such high conductivity causes extremely weak guiding of the metal surface waves (surface plasmons), in disagreement with the observations indicating strong surface wave binding for patterned metal surfaces. In contrast, the strongly bound guided wave solutions for the spoof surface plasmons on a patterned metal surface are essentially the same for a perfect conductor surface and the high conductivity metal surface. For the thin metal hole array on a dielectric surface, the resonances of the spoof surface plasmons converge to those of the surface plasmon, as the hole size is reduced. For a geometrical power transmission of the array of a few percent their first order transmission peaks differ by only a few GHz for THz measurements.

Recently, in order to increase the sensitivity and spectral resolution of THz-TDS measurements, we demonstrated an optical contact technique to characterize high resolution plasmonic resonances in both integral-order and fractional-order SPs [19]–[21].

In this work, in order to better understand THz SSP waves and their excitation mechanism, we experimentally explore the high-resolution THz transmission and reflection properties of a

Manuscript received September 05, 2012; revised November 27, 2012; accepted December 17, 2012. Date of publication February 18, 2013; date of current version February 27, 2013. This work was supported in part by the National Science Foundation (NSF), by the Fundamental Research Funds for the Central Universities, the National Natural Science Foundation of China (NSFC) under Grant 11104360 and Grant 11204191, by the "985 Project" under Grant 98507-010009, and by the "211 Project" of Ministry of Education of China.

Y. Yang is with the School of Science, Minzu University of China, Beijing, 100081, China (e-mail: ypyang_cun@126.com).

D. R. Grischkowsky is with the School of Electrical and Computer Engineering, Oklahoma State University, Stillwater, OK 74078 USA (e-mail: daniel.grischkowsky@okstate.edu).

Color versions of one or more of the figures in this paper are available online at http://ieeexplore.ieee.org.

Digital Object Identifier 10.1109/TTHZ.2013.2241426

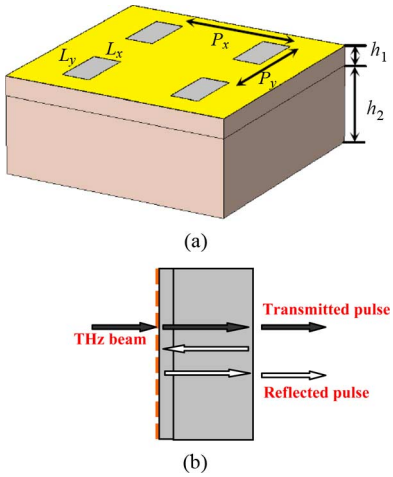

Fig. 1. Schematic diagram of the rectangular hole array in a square lattice with dimensions of $P_x = P_y = 60\ \mu$m, $L_x = 15\ \mu$m, $L_y = 30\ \mu$m, $\mathrm{h}_1 = 420\ \mu$m and $\mathrm{h}_2 = 10$ mm (b) The sample lies in the $x - y$ plane with THz beam incident in the z direction. The Si wafer is in optical contact with the Si plate, consequently there are no reflections at the Si/Si interface between the wafer and the plate. Black arrows show direct transmission. White arrows describe the first reflection from the hole array. Upper white arrow describes the first reflection from the back-side of the Si plate.

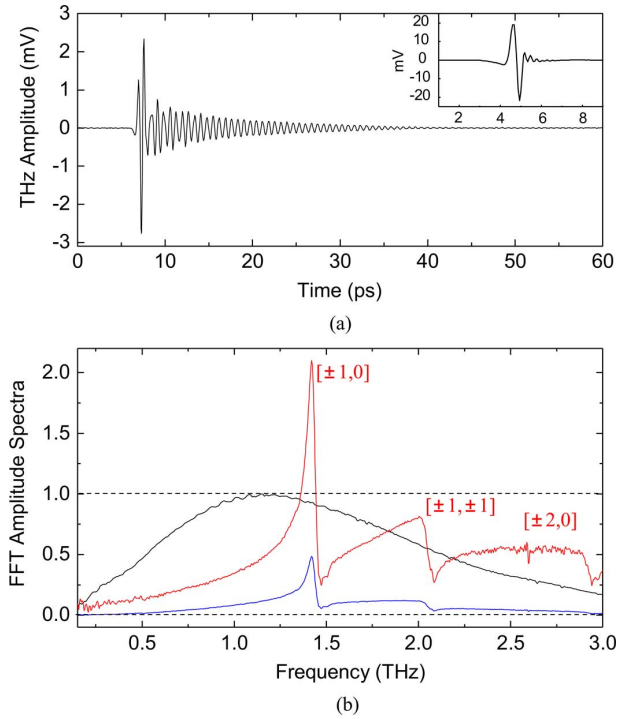

Fig. 2. (a) Measured THz pulse transmitted through the hole array. The measured reference pulse is shown in the inset. The delay of the transmitted pulse through the hole array with respect to the reference pulse is 84 ps. The peak to peak ratio of the reference pulse to the transmitted pulse is approximately 10 (b) Corresponding amplitude spectra. The smooth upper curve is the relative spectrum (normalized to unity) of the reference pulse, which decreases monotonically to 4.5 THz. The lowest curve is the relative spectrum of the transmitted pulse. The stochastic S/N on the transmitted spectrum is 350, but systematic irregular features are significantly larger than stochastic noise. The highly peaked middle curve is the sample spectrum divided by 0.700×0.354 to account for the transmission of the Si and the hole array area fraction. Spectral amplitudes above the dashed line at 1.0 show enhanced transmission.

subwavelength hole array with the most accurate measurements in amplitude and phase to date. In addition, we characterize the reflection at the Si-metal interface using the complex spectral ratio of echo pulse to main pulse, and thereby obtain the first phase shift measurement of the reflection spectrum, as a THz complement to the previous optical studies [22]. These measurements can be compared to spoof surface plasmon theory [15]–[18] to within an accuracy of a few percent. The frequencies of well-defined spectral features have been measured to a precision of 2 GHz for this precise comparison. This work provides the most accurate to date comparison between theory and experiment.

II. Experimental Methods

The $P = 60\ \mu$m square grid of the 38 mm $\times$ 38 mm hole array used in the experiment has submicron precision with the rectangular hole dimensions of 15 μm (x axis) $\times 30\mu$m (y axis). The metallic hole arrays were fabricated by conventional photolithography and metallization processing. A 280-nm-thick Al film was deposited on a double side polished 0.42-mm thick, 51 mm diameter, high-resistivity Si wafer. A 10-mm-thick, 51 mm diameter, high-resistivity Si plate, schematically shown in Fig. 1(a), was placed in optical contact with the backside of the wafer to eliminate the backside reflection, thereby enabling clean observations of plasmon dynamics to 250 ps, corresponding to the frequency resolution of 4 GHz. The arrays are characterized by a photoconductive switch-based broadband THz-TDS system and the sample is placed midway between the photoconductive transmitter and receiver at the confocal beam waist, which increases linearly with wavelength (9 mm diameter for 1 THz) [23]. The input THz pulse, polarized along the x axis, is at normal incidence to the metal face of the sample, as shown in Fig. 1(b).

III. Results and Discussion

A. Experimental Data

The sample is centered within an 18-mm-diameter aperture. The free-space pulse with no sample in place is used as the reference THz pulse shown in the inset of Fig. 2(a), which is much shorter than the damping time of the SSP resonances at metal-film hole array interface. Fig. 2(a) shows the temporal oscillation of the zeroth-order transmitted pulse, where the clean ring-down signal indicates complete optical contact, ensuring complete separation from the backside reflection. The rms noise on the leading edge of the pulse is 0.008 mV, compared to the peak to peak signal strength of 41 mV for the reference pulse, giving the excellent S/N ratio of 5100. The corresponding S/N ratio for the transmitted pulse with peak to peak signal of 5 mV is 625. The total scan length extended to 250 ps, but is not shown in the Fig. 2(a) scan which stops at 60 ps.

The corresponding amplitude spectra of the reference and transmitted pulses are shown in Fig. 2(b). The reference spectrum has been normalized to unity, and with respect to this same normalization the transmitted spectrum is shown as the lower curve. This transmitted spectrum, multiplied by the factor $1/(0.700 \times 0.354)$ to remove the effects of the amplitude transmission of the silicon wafer-plate combination and the array,

is also shown as the upper curve. The spectra region with normalized amplitude above 1.0 shows enhanced transmission. The peak value of 2.1 amplitude enhancement corresponds to enhanced power transmission at 1.421 THz of 4.4 compared to the geometrical transmission. This is equivalent to the enhanced power transmission of 55% compared to the expected 12.5% given by the ratio of the area of the holes compared to the total area (filling factor).

For the transmission spectrum shown in Fig. 2(b), $[m, n]$ designate the specific orders of the SSP mode for a square lattice. The $[\pm 1, 0]$ and $[\pm 1, \pm 1]$ mode SSP resonant peaks were observed at 1.421 and 2.01 THz, whereas the $[\pm 1, 0]$, $[\pm 1, \pm 1]$ and $[\pm 2, 0]$ Wood's anomaly (WA) valleys were observed at 1.472, 2.08, and 2.94 THz, respectively. In particular, the $[\pm 1, 0]$ resonance is the predominant sharp peak with a linewidth of 64 GHz and Q-factor of 22. The frequency red-shift of the $[\pm 1, 0]$ resonance from the Wood's anomaly by 51 GHz indicates the relatively strong coupling of the SSP wave to the metal surface, which is caused by the shapes and filling factor of holes.

At the frequency of the transmission peak, the counter propagating $[\pm 1, 0]$ SSP waves make a standing wave on the metal surface with the nodes and peaks locked to the grid spacing P of 60 μm. In particular, every other peak (adjacent peaks are out of phase by π) is locked to a hole, thereby giving phased coherent transmission in the forward direction. This is the resonance condition for which the wavelength of the guided waves is equal to the grid spacing P (lattice constant) [18]. Consequently, the propagating SSP wavelength is equal to the hole spacing, and the corresponding effective index for the propagating SSP waves is given by the relationship $\lambda = 60\ \mu\text{m} = \lambda_{\text{SSP}}/n_{\text{eff}}$, where λ_{SSP} is the free-space wavelength corresponding to the measured frequency of the SSP resonant peak.

The corresponding slower wave velocity v_p (indicating binding to the surface) is given by $v_p = c/n_{\text{eff}}$. For binding of the SSP wave to the surface, $n_d < n_{\text{eff}}$, and the binding strength increases as $(n_{\text{eff}} - n_d)$ increases. $n_d = \sqrt{\varepsilon_d}$ where ε_d is the dielectric constant of the silicon plate, and $n_d = 3.4175$ for Si [24]. This situation is similar to planar dielectric waveguides, for which the index difference $(n_{\text{eff}} - n_d)$ is a measure of the binding strength of the wave at the dielectric interface. When this difference goes to zero, there is no binding and no guided wave.

For the measured SSP transmission peak of 1.421 THz shown in Fig. 2(b), the effective index is given by $n_{\text{eff}} = \lambda_{\text{SSP}}/\text{P} = 211.1\ \mu\text{m}/60\ \mu\text{m} = 3.518$. Consequently, $(n_{\text{eff}} - n_d) = (3.518 - 3.418) = 0.100$, which is equivalent to $n_{\text{eff}} = n_d(1.030)$, indicating significant binding strength for the SSP with a frequency red-shift of 51 GHz from the Wood's anomaly.

The pulse shown in Fig. 3(a) is the measured zeroth-order first reflected pulse from the back surface of the Si plate and then the front surface of the Si wafer, as shown in Fig. 1(b). Clearly, the polarity of the reflected THz pulse is reversed with respect to that of the transmitted pulse shown in Fig. 2(a). It is interesting to note that the reflected pulse (Region I) is followed by a narrow-band (FWHM of 36 GHz) long-lasting ringing (Region II).The corresponding FFT amplitude spectra of the reflected THz signal in regions I, II, I and II are shown in Fig. 3(b). The

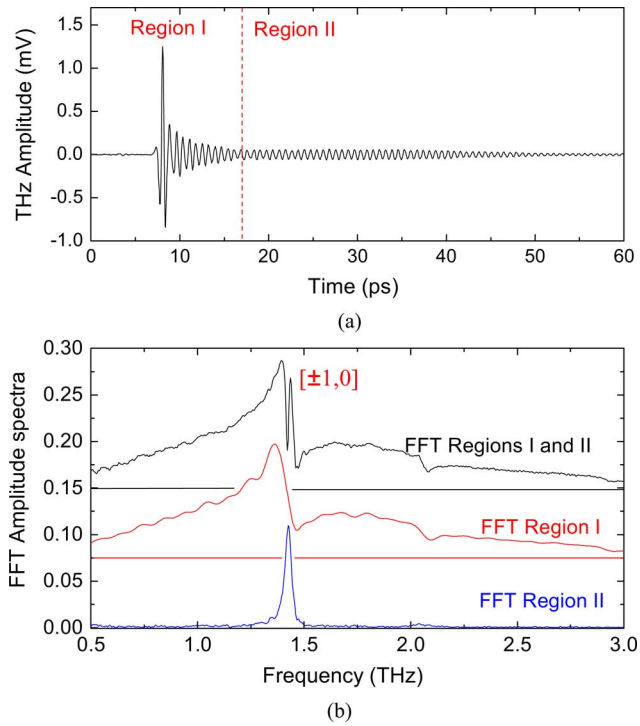

Fig. 3. (a) Zeroth-order first reflected THz pulse, delayed from the transmitted pulse by 237.4 ps, and measured with $S/N = 250$. The vertical dashed line at 17 ps marks the boundary between time Region I and time Region II (b) The corresponding amplitude spectra of the entire reflected pulse (Regions I and II), the initial pulse (Region I), and the long ringing tail (Region II). The amplitude spectra are normalized relative to the measured reference spectrum.

Region-I spectrum is mainly below the fundamental $[\pm 1, 0]$ SSP mode at 1.42 THz, while the Region-II spectrum is predominantly a sharp resonance at 1.435 THz and with a much higher Q-factor $(Q = 39)$; the total spectrum is mainly a combination of Region I and II spectra. Sharp dip at 1.421 THz is in exact overlap with the measured SP resonance at 1.421 THz. However this dip has a much narrower line-width of 12 GHz $(Q = 120)$, compared to that of the peak with FWHM of 64 GHz. A very nicely resolved dip centered on the observed WA valley at 1.472 THz is also shown. This dip is responsible for the double dip structure of the reflection measurement, shown in Fig. 6(a).

B. Transmission Results and Discussion

At normal incidence the resonant SP optical wavelengths for metallic subwavelength holes patterned in square arrays can be approximated as (1) given below [25], assuming that the holes do not perturb the surface propagation (limit as the hole size approaches zero).

$$\lambda_{\text{SP}} = \frac{a}{\sqrt{m^2 + n^2}} \sqrt{\frac{\varepsilon_d \varepsilon_m}{\varepsilon_d + \varepsilon_m}} \tag{1}$$

where m and n are integers corresponding to the specific order of the SP mode, a is the square lattice constant, ε_d and $\varepsilon_m = (\varepsilon_{mr} + i\ \varepsilon_{mi})$ are the dielectric constants of substrate and metal, respectively.

However, for THz frequencies, because of the very high conductivity of metal with $(\varepsilon_d \ll |\varepsilon_{mr}| \ll \varepsilon_{mi})$, the surface wave (SW) is very weakly bound to the metal surface, and (1) ignores the increase in SSP bonding to the metal surface caused by the

actual holes (their size and shape) of the hole array and the thickness of the metal film [15]–[18]. This increase in bonding causes a shift in the THz resonant wavelengths by several percent, as discussed in detail above. To illustrate this point, we evaluate (1) for high conducting metal and obtain the excellent approximation

$$\sqrt{\frac{\varepsilon_d \varepsilon_m}{\varepsilon_d + \varepsilon_m}} \approx \sqrt{\varepsilon_d}\left[1 - \frac{1}{2}\frac{\varepsilon_{mr}\varepsilon_d}{|\varepsilon_m|^2}\right]. \tag{2}$$

For our particular values of $\sqrt{\varepsilon_d} = 3.4175$ for Si [24] and $\varepsilon_{mr} = -3.3 \times 10^4$ and $\varepsilon_{mi} = 6.4 \times 10^5$ for Al at 1 THz [26], this relationship is evaluated to be

$$\sqrt{\frac{\varepsilon_d \varepsilon_m}{\varepsilon_d + \varepsilon_m}} \approx \sqrt{\varepsilon_d}\left[1 + 0.47 \times 10^{-6}\right]. \tag{3}$$

Consequently, in the terahertz domain (1) gives the free-space wavelength λ_{WA} that satisfies Wood's anomaly condition, which gives the transmission minimum [27]

$$\lambda_{WA} = \frac{a}{\sqrt{m^2 + n^2}}\sqrt{\varepsilon_d}. \tag{4}$$

From (4), the $[\pm 1, 0]$ WA valley should occur at 1.463 THz, 9 GHz lower than the measured WA valley at 1.472 THz.

To gain insight into the interaction between the SSP waves and the holes of the grid array, we have carried out calculations based on the finite-element simulations using CST Microwave Studio. As shown in Fig. 4(a), the coupling to the resonant SSP wave is increased with increasing the area of the holes, as shown by the corresponding frequency red-shift of the peak from the observed WA valley at 1.472 THz and broadening of the transmission. For the 25 μm × 50 μm hole, the peak transmission is 0.98. The very strong reduction in shift and amplitude transmission of 10 μm × 20 μm hole size, compared to the 15 μm × 30 μm size should also be noted. As shown in Fig. 4(b), as the filling factor is increased the red-shift of the peak SSP transmission increases slowly, and then between the filling factors of 15%–25%, there is an approximately linear shift with filling factor. Above 25%, the shift increases more slowly and starts to show a saturation-type response.

According to recent in-depth optical SP [28]–[30] and THz SSP [15], [31] studies, the observed red-shift and the asymmetric shape of the $[\pm 1, 0]$ SP and SSP peaks is attributed to Fano-like interference between the directly transmitted wave and a re-emitted wave from the SPs excited on the metal surface.

The simulated behavior of the $[\pm 1, 0]$ WA valley is quite different from the red-shift of the $[\pm 1, 0]$ SP peak, in that the WA valley has a 9 GHz blue-shift to 1.472 THz compared to the calculated value of 1.463 THz from (4). This blue-shift agrees well with the previous reflection measurements in optical and infrared ranges [32], [33], where the WA valleys do not coincide with the predicted minima of the transmission but occur at the frequency where the slope is greatest. In addition, the simulations of Fig. 4(a) show that the WA valley of 1.472 THz does not shift with filling factor.

The excellent agreement between the numerical simulation and measurements (divided by the Si transmission of 0.700) for the amplitude transmission of the hole array is shown in Fig. 5(a) using the square 60 μm grid and the 15 μm × 30μm

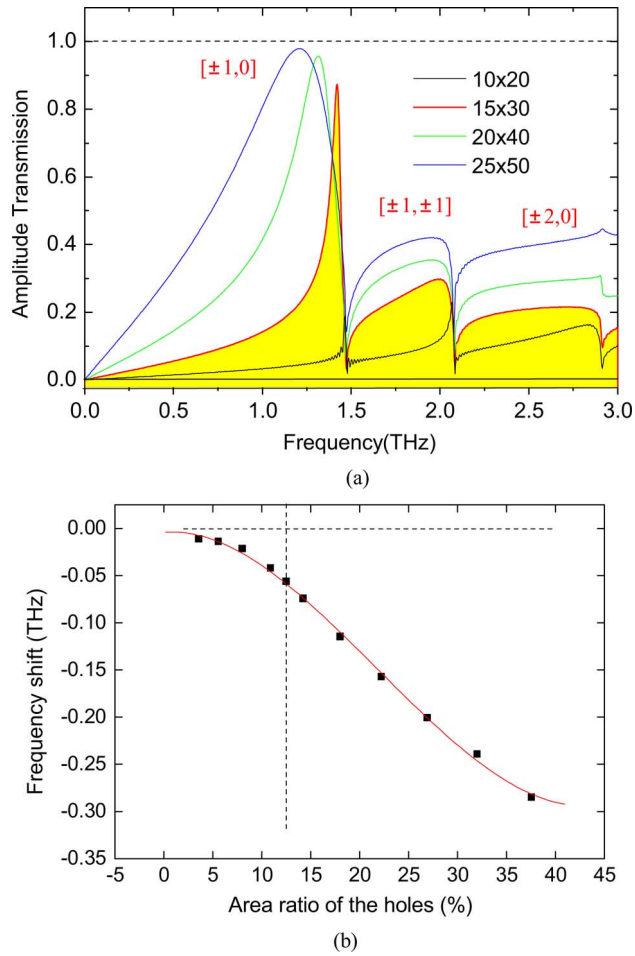

Fig. 4. (a) Calculated amplitude transmission (without normalization by the area ratio) for the square 60 μm grid with different rectangular holes with fixed 1:2 ratio in x, y direction. The highlighted region shows the 15×30 experimental sample. The hole sizes are in μm. (b) Calculated frequency red shift of the peak $[\pm 1, 0]$ SSP mode from the observed WA valley at 1.472 THz as a function of filling factor. The vertical dashed line is for the experimental value of 12.5% with the calculated shift of 54 GHz in good agreement with the observed shift of 51 GHz.

holes with $\varepsilon_d = (3.4175)^2$, and an Al film with the Handbook conductivity of $37.7(\mu\Omega\text{m})^{-1}$ and $\Gamma/2\pi = 10$ THz, for which $\varepsilon = -\sigma_{dc}/(\varepsilon_0\Gamma) + i\sigma_{dc}/(\varepsilon_0\omega)$ [34]. For this high conductivity the calculated transmission is 90%, compared to 100% for the simulation with a perfect conductor. Therefore, these effects are clearly due to THz spoof surface plasmons (SPP) [15]–[18]. The calculated peak of the $[\pm 1, 0]$ SSP mode shown in Fig. 5 is 1.419 THz (1.422 THz for a perfect conductor) and the corresponding minimum occurs at 1.473 THz (same value for perfect conductor), compared to the experimental values of 1.421 and 1.472 THz, respectively. In summary, For Fig. 5(a) the $[\pm 1, 0]$ and $[\pm 1, \pm 1]$ mode SSP resonant peaks were observed at 1.421 and 2.01 THz, and the calculated values were 1.419 and 2.007 THz, whereas the $[\pm 1, 0]$, $[\pm 1, \pm 1]$ and $[\pm 2, 0]$ Wood's anomaly (WA) valleys were observed at 1.472, 2.08, and 2.94 THz, and the calculated values were 1.473, 2.085, and 2.916 THz, respectively. This excellent agreement illustrates both the precision of the experiment and the accuracy of the simulation.

In Fig. 5(b), the corresponding frequency-dependent phase measurements were obtained from the ratio of the complex FFT

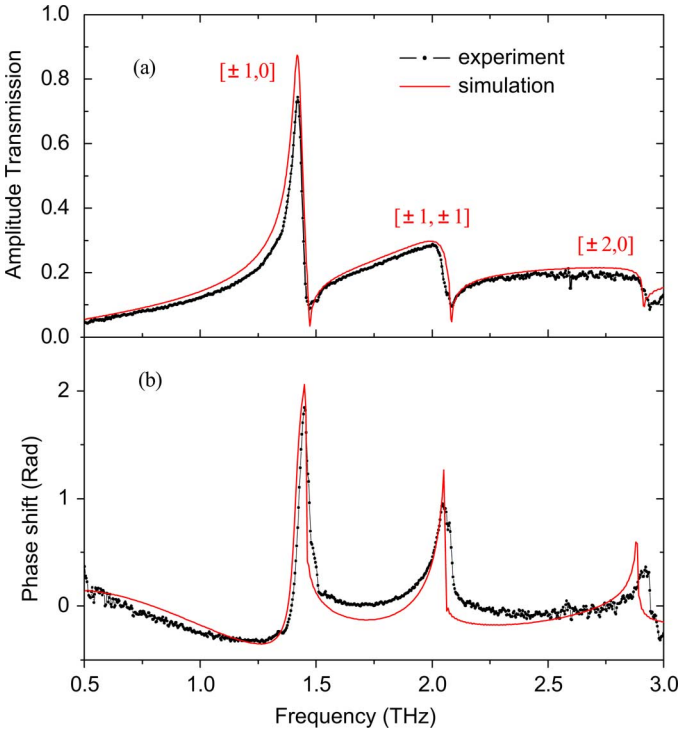

Fig. 5. (a) Measured amplitude transmission for the 15 μm × 30 μm rectangular hole array compared with the simulated transmission (red solid curve) and (b) corresponding phase shifts in radians.

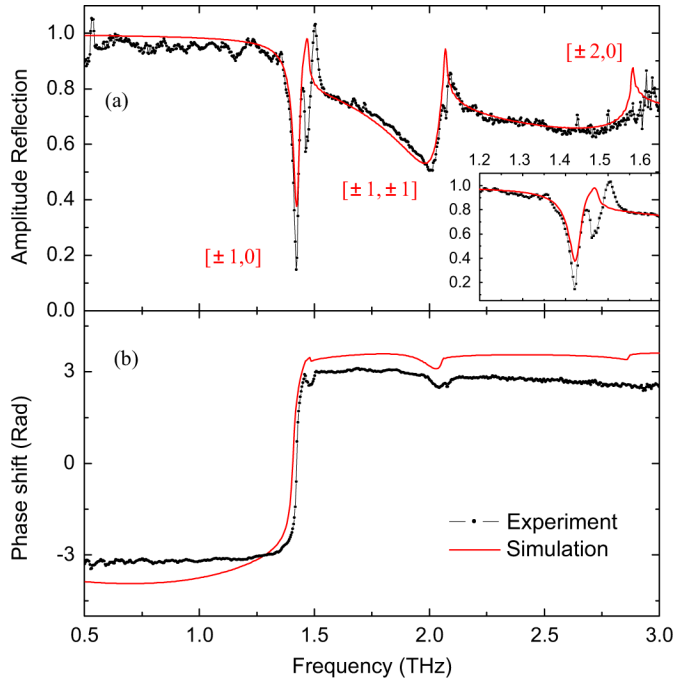

Fig. 6. (a) Measured amplitude reflectivity for the 15 μm × 30 μm rectangular hole array compared with the simulated reflection (red solid curve). The inset is the broad feature in the range of 1.2-1.6 THz and (b) corresponding phase shifts in radians.

of the transmitted pulse divided by the reference pulse. For this case, the starting positions of the pulses are adjusted to be the same in the digital data to eliminate the corresponding large phase sweep. Consequently, the measured phase changes in the transmission could be obtained directly in this case without concern for unwinding due to the 2π phase shift inherent in the numerical processing. The comparison between simulation and experiment is considered to be quite good. A common feature is the resulting phase changes are localized and surprisingly look like a resonant absorption line. This feature is due to the Fano lineshape [15]–[18], [31], which is known to produce this type of phase response.

C. *Reflection Results and Discussion*

The amplitude reflectivity at the Al–Si interface was obtained by dividing the amplitude spectrum of the reflected pulse by the amplitude spectrum of the transmitted pulse, which was multiplied by the frequency-independent reflection coefficient at the Si-air interface $\mathrm{R_{Siair}} = (n-1)/(n+1) = 0.547$. The absorption of high-resistivity Si is negligible over our frequency range for a path length of 2 cm and the index of refraction is $n = 3.4175 \pm 0.00005$ and can be considered frequency independent [24]. The experimental amplitude reflectivity, shown in Fig. 6(a) by the experimental dots connected by a line, show scatter due to small frequency variations in the experimental system for the two different measurements, which are then divided one by the other and thereby these variations are enhanced. However, the main features are clearly evident with good agreement with the simulation with one notable exception to be discussed below.

Firstly, the sharp minimum for the experiment occurs at 1.421 THz and amplitude of 0.13, compared to simulation at 1.422 THz and amplitude of 0.33. Note that the $[\pm 1, 0]$ measured SSP peak occurs at 1.421 THz. Secondly, the experiment shows a second dip at 1.461 THz, quite close to the 1.463 THz predicted by (4), and in contrast the simulation shows a peak at 1.47 THz. Note that the WA dip in transmission occurred at 1.472 THz (experiment) and 1.473 THz (simulation). The experiment also shows a sharp well-defined peak at 1.505 THz.

According to SSP and WA theories, the incident THz electromagnetic waves will strongly couple to counter-propagating THz-SSP waves at the SSP resonant frequency, and the THz waves will also be strongly diffracted along the surface of the grating at the WA wavelength, determined by the grating periodicity, thereby giving rise to the reflection minima. It is important to note, that assuming no Ohmic loss in the metal film, a measure of the power loss from the measured zeroth-order direction, due to first-order and higher order diffraction by the two-dimensional grating of the hole-array, is the quantity $\mathrm{PLD} = 1-(\mathrm{T}+\mathrm{R})$, where T and R are the square of the amplitude transmission and reflection curves. Such strong diffraction could be a possibility to explain the mystery dip. Recent work has shown the importance of first-order diffraction to transmission measurements made in the zeroth-order direction [20], [21].

The relative phase shift of the reflected pulse, shown in Fig. 6(b), also shows good general agreement with the simulation. To obtain these results, the pulses were first numerically overlapped in time to eliminate the linear phase shift due to silicon wafer and plate and then the complex Fourier transforms were made. Here, in the frequency range from 0.5 to 1.4 THz, the phase shift is relatively independent of frequency and close

to the value of -3.14, corresponding our adjusting of the very low-frequency phase to converge to $-\pi$ to obtain the mirror polarity reversal of the THz pulse, while giving the region from $-\pi$ to π to be accessible without the numerical 2π phase jump. Clearly, there is an unusual continuous (involving many data points) step-like 2π phase shift at the resonant frequency 1.42 THz, due to strongly modulated amplitude of the reflection. After the 2π phase shift the mirror response gives phase reversal of the frequency components, together with relatively small phase changes corresponding to the features seen in the amplitude reflection. However, the small dip at 1.49 THz still needs explanation.

IV. Conclusion

In summary, by using high-resolution THz-TDS, we have performed the most accurate measurement to date of the amplitude and phase of the frequency-dependent transmission and reflection of a thin metal hole-array on high-resistivity silicon plate. For the $[\pm 1, 0]$ THz spoof surface plasmon transmission peak our measurement agreed with numerical simulation to within 2 GHz and for the associated minimum the agreement was within 1 GHz. For the $[\pm 1, 0]$ spoof surface plasmon reflection deep-minimum, our measurement agreed with simulation to 1 GHz, but an associated second shallow minimum at the Wood's anomaly was observed, that was not shown in the simulation. In addition, we have shown that the red-shift of the $[\pm 1, 0]$ SSP transmission peak from the observed WA dip indicates the coupling strength of the SSP wave to the metal surface, and provides a measurement of the SSP wave velocity.

Acknowledgment

The authors acknowledge experimental support from A. J. Shutler.

References

[1] R. Ulrich, "Far-infrared properties of metallic mesh and its complementary structure," *Infrared Phys.*, vol. 7, pp. 37–55, 1967.

[2] C. C. Chen, "Transmission through a conducting screen perforated periodically with apertures," *IEEE Trans. Microw. Theory Techn.*, vol. MTT-18, no. 9, pp. 627–632, Sep. 1970.

[3] F. Keilmann, "Infrared high-pass filter with high contrast," *Int. J. Infrared Millim. Waves*, vol. 2, pp. 259–272, 1982.

[4] C. M. Rhoads, E. K. Damon, and B. A. Munk, "Mid-infrared filters using conducting elements," *Appl. Opt.*, vol. 21, pp. 2814–2816, 1982.

[5] C. Winnewisser, F. Lewen, J. Weinzierl, and H. Helm, "Transmission features of frequency-selective components in the far-infrared determined by terahertz time-domain spectroscopy," *Appl. Opt.*, vol. 38, pp. 3961–3967, 1999.

[6] T. W. Ebbesen, H. J. Lezec, H. F. Ghaemi, T. Thio, and P. A. Wolff, "Extraordinary optical transmission through sub-wavelength hole arrays," *Nature*, vol. 391, pp. 667–669, 1998.

[7] D. Qu, D. Grischkowsky, and W. Zhang, "Terahertz transmission properties of thin subwavelength metallic hole arrays," *Opt. Lett.*, vol. 29, pp. 896–898, 2004.

[8] K. Azad and W. Zhang, "Resonant terahertz transmission in subwavelength metallic hole arrays of sub-skin-depth thickness," *Opt. Lett.*, vol. 30, pp. 2945–2947, 2005.

[9] K. Azad, Y. Zhao, and W. Zhang, "Effect of dielectric properties of metals on terahertz transmission in subwavelength hole arrays," *Opt. Lett.*, vol. 31, pp. 2637–2639, 2006.

[10] Y. Yang, R. Singh, and W. Zhang, "Anomalous terahertz transmission in bowtie plasmonic antenna apertures," *Opt. Lett.*, vol. 36, pp. 2901–2903, 2011.

[11] T. Matsui, A. Agrawal, A. Nahata, and Z. V. Vardeny, "Tranmission resonances through aperiodic arrays of subwavelength apertures," *Nature*, vol. 446, pp. 517–521, 2007.

[12] J. W. Lee, T. H. Park, P. Nordlander, and D. M. Mittleman, "Optimum areal coverage for perfect transmission in a periodic metal hole array," *Appl. Phys. Lett.*, vol. 97, 261112, 2010.

[13] H. Cao and A. Nahata, "Influence of aperture shape on the transmission properties of a periodic array of subwavelength apertures," *Opt. Express*, vol. 12, pp. 3664–3672, 2004.

[14] F. Miyamaru, Y. Sasagawa, and M. W. Takeda, "Effect of dielectric thin films on reflection properties of metal hole arrays," *Appl. Phys. Lett.*, vol. 96, 021106, 2010.

[15] J. B. Pendry, L. Martin-Moreno, and F. J. Garcia-Vidal, "Mimicking surface plasmons with structured surfaces," *Sci.*, vol. 35, pp. 847–848, 2004.

[16] F. J. Garcia-Vidal, L. Martin-Moreno, and J. B. Pendry, "Surfaces with holes in them: new plasmonic metamaterials," *J. Opt. A: Pure Appl. Opt.*, vol. 7, pp. S97–S101, 2005.

[17] F. J. G. de Abajo and J. J. Saenz, "Electromagnetic surface modes in structured perfect-conductor surfaces," *Phys. Rev. Lett.*, vol. 95, p. 233901, 2005.

[18] F. J. G. de Abajo, "Colloquium: Light scattering by particle and hole arrays," *Rev. Mod. Phys.*, vol. 79, pp. 1267–1290, 2007.

[19] D. Qu and D. Grischkowsky, "Observation of a new type of a thz resonance of surface plasmons propagating on metal-film hole arrays," *Phys. Rev. Lett.*, vol. 93, p. 196804, 2004.

[20] Y. Yang and D. Grischkowsky, "Understanding fractional order surface plasmons," *Opt. Lett.*, vol. 36, pp. 4218–4220, 2011.

[21] Y. Yang and D. Grischkowsky, "The 4-step pulses of fractional-order surface plasmons," *Opt. Lett.*, vol. 37, pp. 1709–1711, 2012.

[22] E. Altewischer, M. P. v. Exter, and J. P. Woerdman, "Nonreciprocal reflection of a subwavelenth hole array," *Opt. Lett.*, vol. 28, pp. 1906–1908, 2003.

[23] D. Grischkowsky, S. Keiding, M. van Exter, and C. Fattinger, "Far-infrared time-domain spectroscopy with terahertz beams of dielectrics and semiconductors," *J. Opt. Soc. Amer. B*, vol. 7, pp. 2006–2015, 1990.

[24] J. Dai, J. Zhang, W. Zhang, and D. Grischkowsky, "THz time -domain spectroscopy characterization of the far-infrared absorption and index of refraction of high resitivity, float-zone silicon," *J. Opt. Soc. Amer. B.*, vol. 21, pp. 1379–1386, 2004.

[25] H. F. Ghaemi, T. Thio, D. E. Grupp, T. W. Ebbesen, and H. J. Lezec, "Surface plasmons enhance optical transmission through subwavelength holes," *Phys. Rev. B*, vol. 58, pp. 6779–6782, 1998.

[26] W. Ehrenberg, *Electric Conduction in Semiconductors and Metals*. Clarendon, Oxford, U.K.: , 1958.

[27] L. Rayleigh, "On the dynamical theory of gratings," *Proc. Roy. Soc. Lond. A*, vol. 79, pp. 399–416, 1907.

[28] C. Genet, M. P. van Exter, and J. P. Woerdman, "Fano-type interpretation of red shifts and red tails," *Opt. Commun.*, vol. 225, pp. 331–335, 2003.

[29] M. Sarrazin, J.-P. Vigneron, and J.-M. Vigoureux, "Role of wood anomalies in optical properties of thin metallic films with a bidimensional array of subwavelength holes," *Phys. Rev. B*, vol. 67, 2003, 085415.

[30] M. M. J. Treacy, "Dynamical diffraction explanation of the anomalous transmission of light through metallic gratings," *Phys. Rev. B*, vol. 66, 195105, 2002.

[31] J.-B. Masson, A. Podzorov, and G. Gallot, "Extended Fano model of extraordinary electromagnetic transmission through subwavelength hole arrays in the terahertz domain," *Opt. Express*, vol. 17, pp. 15280–15291, 2009.

[32] H. Palmer, "Parallel diffraction grating anomalies," *J. Opt. Soc. Amer.*, vol. 42, pp. 269–276, 1952.

[33] J. E. Stewart and W. S. Gallaway, "Diffraction anomalies in grating spectrophotometers," *Appl. Opt.*, vol. 1, pp. 421–430, 1962.

[34] Y. Zhao and D. R. Grischkowsky, "2-D terahertz metallic photonic crystals in parallel-plate waveguides," *IEEE Trans. Microw. Theory Techn.*, vol. 55, pp. 656–663, 2007.

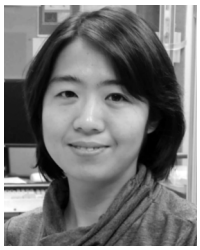

Yuping Yang received the B.S. and M.S. degrees from Capital Normal University, Beijing, China, in 1999 and 2002, and the Ph.D. degree from Institute of Physics, Chinese Academy of Science, Beijing, China, in 2005.

In 2005, she joined the School of Science, Minzu University of China, Beijing, China. From Sep., 2010 to Aug., 2011, she spent one year as a Visiting Scholar at the Ultrafast Terahertz Research Group (UTRG) at Oklahoma State University, Stillwater, USA. Her current research interests include terahertz time-domain detection, terahertz surface plasmon, and terahertz metamaterials.

Daniel R. Grischkowsky (SM'90–F'92) received the B.S. degree from Oregon State University, Corvallis, OR, USA, in 1962, and the Ph.D. degree from Columbia University, New York, NY, USA, in 1968.

In 1969, he joined the IBM T. J. Watson Research Center, Yorktown Heights, NY, USA. In 1993, he joined Oklahoma State University, where his work has concentrated on unique applications of THz-TDS, including waveguides, the Sommerfeld wave, surface waves, hole arrays and photonic crystals.

Dr. Grischkowsky is a Fellow of the Optical Society of America (OSA) and the American Physical Society. He was awarded the 1985 Boris Pregel Award by the NY Academy of Sciences, the OSA 1989 R. W. Wood Prize, the OSA 2003 William F. Meggers Award, and the 2011 Kenneth J. Button Prize from the International Society of IR, MM, and THz waves.